Reflectance Computation for a Specular Only V-Cavity

Dorian Saint-Pierre[1(✉)], Lionel Simonot[1,2], and Mathieu Hébert[1]

[1] Université de Lyon, UJM-Saint-Etienne, CNRS, Institut D'Optique Graduate School, Laboratoire Hubert Curien UMR 5516, Saint-Etienne, France
dorian.saint.pierre@univ-st-etienne.fr
[2] Université de Poitiers, Institut Prime UPR CNRS 3346, Futuroscope Chasseneuil, Poitiers, France

Abstract. The color of a surface structured at the mesoscopic scale differs from the one of a flat surface of the same material because of the light interreflections taking place in the concavities of the surface, as well as the shadowing effect. The color variation depends not only on the surface topology but also on the spectral reflectance of the material, its matte or glossy finishing, and the angular distribution of the incident light. For an accurate prediction of the radiance perceived from each point of the object by an observer or a camera, we must take into account comprehensively the multiple paths of light which can be reflected, scattered or absorbed by the material and its surface. In this paper, we focus on the light reflection component due to the material-air interface, in the special case of a surface structured with parallel, periodical, specular V-shaped ridges, illuminated either by collimated light from any direction of the hemisphere, or by diffuse light. Thanks to an analytical model, we compute the radiance reflected in every direction of the hemisphere by accounting for the different interreflections, according to the angular reflectance of the panels and the aperture angle of the cavity. We can then deduce the apparent reflectance of the cavity when viewed from a large distance.

Keywords: Surface reflection · Light interreflections · Reflectance model

1 Introduction

It is well known that the structure of surfaces and materials has a crucial influence on the way they reflect light, thereby on their appearance. A same material structured in different ways can yield very different appearance attributes, from bright to dark, glossy to matte or transparent to opaque.

The influence of the material structure on appearance is mainly related to concept of light scattering, a concept which covers a wide variety of optical principles according to the size of the material structures and their periodicity. Regular or periodical structures whose characteristic size is comparable to the wavelength of light generate interferences or diffraction, and consequently colorations which are often called structural colors [1]. These effects have been widely explored in optics for more than one century, even though pseudo-periodical structures are still an active subject of investigation [see

S. Tominaga et al. (Eds.): CCIW 2019, LNCS 11418, pp. 289–303, 2019.
https://doi.org/10.1007/978-3-030-13940-7_22

for example Ref. 2]. In opposition, irregular structures can generate both coherent and incoherent light scattering which mainly results in a reorientation of light in space and depolarization. For these randomly microstructured materials, many models have also been proposed in the last century to predict their reflection and transmission properties according to the wavelength, polarization, orientation and position of light. Among the most famous theories for the light scattering by volumes, we can mention the Kubelka-Munk model initially introduced for paints [3], the Melamed model for pigments powders and slurries [4], the radiative transfer theory by Chandrasekhar [5], the multi-flux theory, the Van de Hulst works for scattering by particles [6], etc. We can also evocate famous models for the scattering of light by surfaces with a random roughness, from Beckman and Spizzichino [7] who modelled diffraction by such surfaces, through Torrance and Sparrow [8] who modelled incoherent reflection by randomly organized microfacets, to the most advanced models which also take into account the multiple scattering between different facets [9–11]. All these models form a large prediction toolbox for many visual attributes (color, translucency and opacity, gloss and matt aspect), applicable to a wide range of materials according to their optical properties (refractive indices, scattering and absorption coefficients…) and structural properties (surface roughness, particle size and concentration, layer thickness…), provided the material can be considered as homogeneous at the macro- or mesoscopic scale.

However, for many kinds of surfaces or objects, the multiscale structure of the matter do have to be taken into account in order to obtain accurate optical models and appearance predictions. Describing scattering at multiple scales is generally done by combining different models. The classical literature in physics shows various examples. Mie scattering model is used to describe the light scattering by one particle, and a radiative transfer model is then used to describe the light transport through a piece of medium with particles. For stacks of diffusing layers, the Kubelka-Munk model describes the light scattering at the microscopic scale within each layer and predicts its reflectance and transmittance, then the Kubelka layering model [12] or more advanced models describe the flux transfers at the mesoscopic scale between the different layers with their respective interfaces [13, 14]. For halftone prints, the optical properties of the paper and the inks can be both modeled by the Kubelka-Munk theory [15], then the scattering properties of the set of ink dots on top of the paper can be predicted by a number of models describing the flux transfers between the different inked and non-inked areas [16–19]. But models are still missing for a volume made of an alternation of mesoscopic bricks of materials and the 3D flux transfers taking place between them, as we can find in 3D inkjet printing, and for a surface whose shape has been given a mesoscopic, possibly periodical structure.

In the latter case on which the present paper is focused, the multiple reflections between the different areas of the non-flat surface, also called interreflections, give to the object specific reflection properties according to the illumination conditions that the models mentioned above cannot render properly. As shown in recent studies dedicated to ridged Lambertian materials (ridges with V-profile) [20, 21], the presence of periodical ridges modifies the color of the material in comparison to the color of the flat surface, in different ways according to the ridge aperture and the illumination conditions: the color of the ridge surface is brighter and more saturated than the one of the flat surface under frontal collimated illumination, but it is darker and less saturated

under diffuse illumination. Interreflection models taking explicitly into consideration the microscopic optical properties of the material and the mesoscopic structure of the surface are capable to predict these color variations, thus also allowing the prediction of the irradiance repartition at these two scales. The present paper follows this investigation on materials with periodical V-shaped ridges under different illumination conditions, by considering this time a nonscattering material and describing the multiple specular reflections undergone by each ray between faces of the structure, behaving like mirrors. As for the model dedicated to Lambertian materials, we adopt a radiometric approach, yielding analytical expressions for the angular and bi-hemispherical reflectance of the structured surface, as a function of the material refractive index and the ridge aperture α (see Fig. 1).

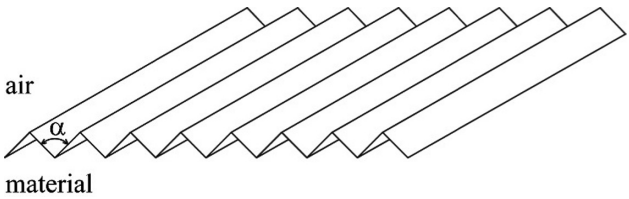

Fig. 1. Structured surface with parallel and periodical V-shaped ridges of aperture angle α.

The paper is structured as follows: we first present the useful concepts for describing our model, to then introduce the formalization of multiple light reflections happening in a V-cavity, with specular surfaces as pannels. After this we move on to the fourth section where we present the results obtained by using the presented model, and we end with our conclusions.

2 Reflectance

The fraction of light reflected by the structured surface is characterized by the *reflectance* concept, which is defined for an area of the surface much larger than the width of the cavities. This concept relies on radiometric quantities related to the amount of incident and reflected light, recalled below, which can also be used to describe the multiple reflection process within each cavity.

The light power, or flux, denoted as F, can be regarded as a collection of light rays propagating from the source to the objects, then from areas of the objects to other areas, then from the objects to the observer. The distribution of the light flux over a given surface is described by the concept of *irradiance* (for incoming light) or *exitance* (for outgoing light), defined as the density of received or emitted flux dF per elementary area dA:

$$E = \frac{dF}{dA} \tag{1}$$

Radiance, denoted as L, is defined by the density of light power (or flux) d^2F per elementary geometrical extent d^2G:

$$L = \frac{d^2F}{d^2G} \tag{2}$$

where the geometrical extent defines the flux transfer volume between the two elementary areas.

Reflectance denotes any ratio of reflected flux to incident flux relative to the same surface element, defined for a given illumination and observation geometry. In this paper, reflectance is generically denoted as R. In the special case of air-medium interfaces, the angular reflectance is denoted as $R_{01}(\theta)$ for collimated light coming from medium 0 (in our case, it is air, of refractive index $n_0 = 1$) at the interface with medium 1 (of refractive index n_1, which can be either real or complex), with an angle of incidence θ. The term n denotes the relative optical index of the interface, i.e., the ratio of the refractive indices as follows:

$$n = \frac{n_1}{n_0} \tag{3}$$

When a light ray with radiance L_i is reflected on a flat interface, the reflected radiance L_r is simply given by:

$$L_r = R_{01}(\theta)L_i \tag{4}$$

where θ is the angle between the incident radiance and the normal of the interface.

3 Multiple Reflections of a Light Ray in a Specular Cavity

We can notice from Fig. 1 that a light ray entering into one cavity is reflected, possibly multiple times, in this cavity only. Therefore, we can focus on the reflection of light by one cavity, and consider that all cavities reflect light in the same way. In this section, we propose to present the analytical model permitting to accurately predict the amount and directions of light reflected by the cavity. The model is based on geometrical optics, with an approach comparable to ray tracing. It describes the path of the light after the different reflections across the structure, and takes into account the precise number of bounces that the light undergoes on the panels.

3.1 Geometry of the Cavity

Each cavity is formed by two specular panels of infinite length along the x axis of the 3D Cartesian space (Fig. 2). The width of both panels is set to unity (it could be equivalently any other value: the width has no impact on the interreflection phenomenon as shown in [18] and on the computation of the specular radiance that we want to perform here). The angle between the two panels, also called “aperture of the

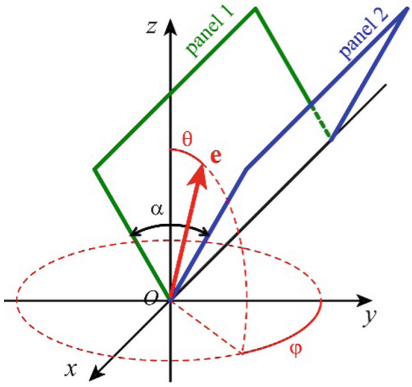

Fig. 2. 3D geometry of one cavity, and vector **e** representing the direction of illumination.

cavity", is denoted as α. Hence, each panel forms a dihedral angle α/2 with the *(xOz)*-plane, where the z axis corresponds to the normal of the average structured surface.

The normal of panels 1 and 2 are respectively:

$$\mathbf{N_1} = \begin{pmatrix} 0 \\ \cos(\alpha/2) \\ \sin(\alpha/2) \end{pmatrix} \quad \text{and} \quad \mathbf{N}_2 = \begin{pmatrix} 0 \\ -\cos(\alpha/2) \\ \sin(\alpha/2) \end{pmatrix} \tag{5}$$

The incident light ray is characterized by unit radiance, and a unit vector **e** with spherical coordinates (θ, φ) represented in Fig. 2. In this Cartesian coordinate system, the vector **e** is given by:

$$e = \begin{pmatrix} \sin\theta \sin\varphi \\ \sin\theta \cos\varphi \\ \cos\theta \end{pmatrix} \tag{6}$$

3.2 Multiple Reflections in a Cavity

Once a light ray enters into a cavity, it may undergo one or several successive reflections on the panels. After each reflection, the direction of the ray is modified according to Snell's laws. However, in geometrical optics, it is classical to represent the image of the ray reflected by a mirror which is aligned with the incident ray, as shown on the left of Fig. 3 through the example of two rays. By using this representation for the cavity, we can draw a straight line aligned with the incident ray, crossing the successive images of the panels: after a reflection on panel 1, the ray reaches the image of panel 2 (which forms an angle α with panel 1), then the image of panel 1 (which also forms an angle α with the image of panel 2, and so on).

The number of reflections depends on both orientation and position of the ray. This is visible in Fig. 3 where the two rays are parallel (thus characterized by the same

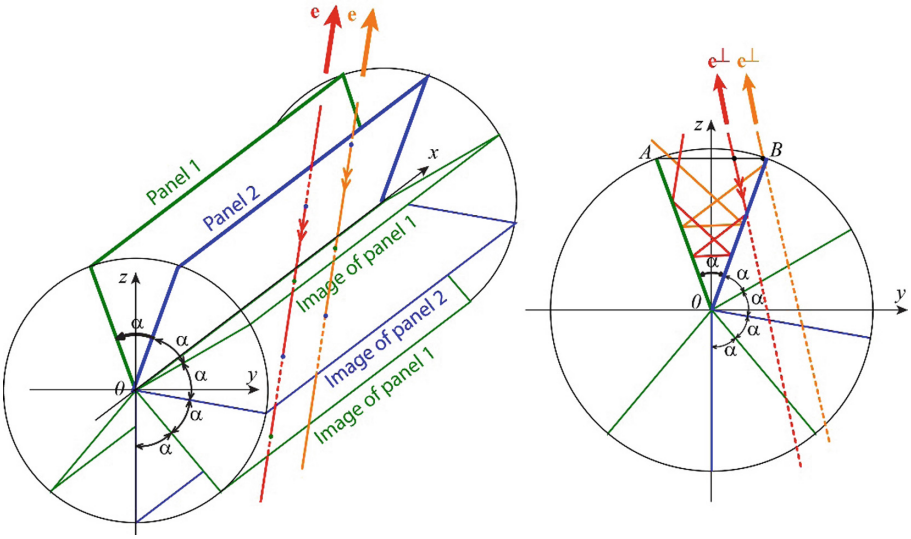

Fig. 3. Left: 3D representation of two parallel light rays oriented according to a same vector **e** striking the cavity in different positions on panel 2. Right: 2D representation of the two same light rays projected onto the (yOz) vertical plane. The light path can be represented by a straight line meeting the successive images of the panels from each other. The projection of real light paths in broken straight lines is also represented on the figure (left).

vector **e**) and strike panel 2 in different positions: one ray (represented in red) undergoes 4 reflections, whereas the other ray undergoes 3 reflections. The ray light paths in broken straight lines are featured on the right of the figure, in a projection onto the ($y0z$) plane of the 3D scene represented on the left of the figure. In this plane, the projection of vector **e**, denoted as $\mathbf{e}^{\perp}$, is:

$$\mathbf{e}^{\perp} = \begin{pmatrix} \sin\theta' \\ \cos\theta' \end{pmatrix}$$

with

$$\theta' = \arctan(\tan\theta\cos\varphi) \tag{7}$$

3.3 Number of Reflections

The number of reflections according to the orientation and position of the ray is computed according to the following geometrical considerations, in the (yOz) plane.

The orientation of the ray is denoted by the angle θ' given by Eq. (7). Its position is described by the point P where the ray meets the line (AB) which joins the extremities of the panels in the (yOz) plane, drawn in Fig. 4. This point P has the coordinates

$P = (y_P, \cos(\alpha/2))$. The ray meets the unit circle centered in point $O = (0, 0)$ in two points: first in point $G = (\sin\beta_G, \cos\beta_G)$, then in point $H = (\sin\beta_H, \cos\beta_H)$.

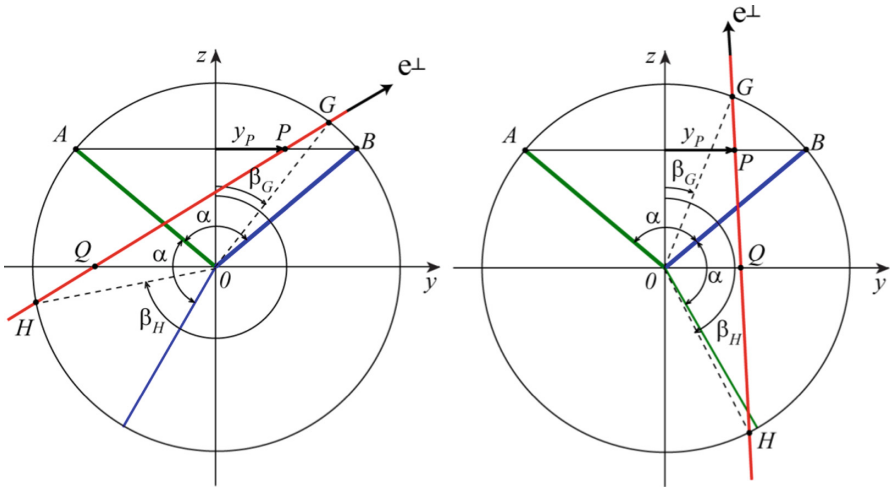

Fig. 4. Geometry for the calculation of the number of reflections, for a same position y_P of the ray, and two different orientations.

Figure 4 shows two examples for the same position y_P but two different orientations of the ray. On the left of the figure, the ray strikes first panel 1, on the right of the figure, it strikes first panel 2. The panel first met is determined by the following condition: if the meeting point $Q = (y_q, 0)$ of the ray and the y-axis has a negative abscissa y_q, panel 1 is met first, otherwise, panel 2 is met first. With some geometrical calculation, we find that abscissa y_q is given by

$$y_q = \frac{\sin(\beta_H - \beta_G)}{\cos\beta_G - \cos\beta_H} \tag{8}$$

where the angles β_G and β_H are computed as follows.

Since $\overrightarrow{PG} = \left(\sin\beta_G - y_P, \cos\beta_G - \cos\left(\frac{\alpha}{2}\right)\right)$ and $\mathbf{e}^{\perp}$ are collinear, we have:

$$\det\begin{pmatrix} \sin\beta_G - y_P & \sin\theta' \\ \cos\beta_G - \cos\left(\frac{\alpha}{2}\right) & \cos\theta' \end{pmatrix} = 0 \tag{9}$$

After some calculation, Eq. (9) can be written

$$\sin(\beta_G - \theta') = y_P \cos\theta' - \cos\left(\frac{\alpha}{2}\right)\sin\theta' \tag{10}$$

and by noticing that $\beta_G - \theta' < \pi/2$, we obtain

$$\beta_G = \theta' + \arcsin\left[y_P \cos\theta' - \cos\left(\frac{\alpha}{2}\right)\sin\theta'\right] \tag{11}$$

Likewise $\overrightarrow{PH}$ and $\mathbf{e}^{\perp}$ are collinear, and by following similar reasoning as above with point H in place of point G, therefore with angle β_H in place of β_G, we obtain

$$\sin(\beta_H - \theta') = y_P \cos\theta' - \cos\left(\frac{\alpha}{2}\right)\sin\theta' \tag{12}$$

This time, we can notice that $\beta_H - \theta' > \pi/2$, therefore we have:

$$\beta_H = \theta' + \pi - \arcsin\left[y_P \cos\theta' - \cos\left(\frac{\alpha}{2}\right)\sin\theta'\right] \tag{13}$$

Figure 4 illustrates the fact that β_H is a reflex angle, i.e., higher than π, when the ray strikes first panel 1 ($y_q < 0$), and a salient angle, i.e., lower than π, when it strikes first panel 2 ($y_q > 0$). We may prefer using the angle γ_H, obtuse in any case, defined as:

$$\gamma_H = \begin{cases} 2\pi - \beta_H \text{ when } y_q < 0 \\ \beta_H \text{ when } y_q > 0 \end{cases} \tag{14}$$

Finally, the number of reflections occurring after the first reflection of the first panel met is the number of times angle $\gamma_H - \alpha/2$ contains α. Hence, the total number of reflections is given by

$$m = \text{floor}\left[\frac{\gamma_H}{\alpha} - \frac{1}{2}\right] + 1 \tag{15}$$

where symbol floor[.] gives the integral part of the number in argument.

3.4 Radiance Attenuation for One Ray

Now that the number of light reflections has been determined, we can express the global attenuation undergone by the radiance, by multiplying the successive Fresnel reflectances $R_{12}(\theta_i)$ corresponding to the different reflections. For each reflection, we need to compute the local incidence angle θ_i. This local incidence angle can be easily obtained through the dot product between vector $\mathbf{e}$, which describes the direction of the ray, and the normal of the panel, or image of panel, on which the considered reflection occurs.

The panels have the normal vectors $\mathbf{N}_1$ and $\mathbf{N}_2$ given by Eq. (5). The local incident angle for the first reflection depends on whether the ray first meets panel 1 or panel 2, therefore on the sign of the parameter y_q defined by Eq. (8):

$$\theta_i = \begin{cases} \arccos(\mathbf{e} \cdot \mathbf{N_1}) \text{ if } y_q < 0 \\ \arccos(\mathbf{e} \cdot \mathbf{N}_2) \text{ if } y_q > 0 \end{cases} \tag{16}$$

where the symbol "·" denotes the dot product

The following reflections, if any, occur on images of panels whose normal vector denoted as $\mathbf{N}_1^{(j)}$ or $\mathbf{N}_2^{(j)}$ if the first reflection occurs on panel 1, respectively on panel 2. These normal vectors, for $j = 2$ to the number of reflections m given by Eq. (15), are defined as

$$\mathbf{N}_1^{(j)} = \begin{pmatrix} 0 \\ \cos(\alpha/2 + (j-1)\alpha) \\ \sin(\alpha/2 + (j-1)\alpha) \end{pmatrix} \quad \text{and} \quad \mathbf{N}_2^{(j)} = \begin{pmatrix} 0 \\ -\cos(\alpha/2 + (j-1)\alpha) \\ \sin(\alpha/2 + (j-1)\alpha) \end{pmatrix} \tag{17}$$

and the local incident angle is given by

$$\theta_i^{(j)} = \begin{cases} \arccos\left(\mathbf{e} \cdot \mathbf{N}_1^{(j)}\right) & \text{if } y_q < 0 \\ \arccos\left(\mathbf{e} \cdot \mathbf{N}_2^{(j)}\right) & \text{if } y_q > 0 \end{cases} \tag{18}$$

Finally, the global attenuation of the radiance according to its position y_P between $-\sin(\alpha/2)$ and $\sin(\alpha/2)$ and its orientation (θ, φ), is given by the reflectance:

$$R(\theta, \varphi, y_P) = \prod_{j=1}^{m} R_{01}\left[\theta_i^{(j)}\right] \tag{19}$$

where $\theta_i^{(1)}$ denotes the local angle θ_i for the first reflection given by Eq. (16).

Notice that according to the Helmholtz reciprocity principle, a ray following the same path within the cavity but in opposite direction would undergo exactly the same attenuation. Hence, $R(\theta, \varphi, y_P)$ can denote the attenuation for the ray coming or exiting the cavity at the angle (θ, φ) through the position y_P.

4 Reflectance of the Structured Surface

From the reflectance attached to each incident ray within the cavity, we can derive the reflectance of the structured surface for a Lambertian illumination. It can be a hemispherical-directional reflectance, also called angular reflectance, being a function of the observation direction. Another interesting type is the bi-hemispherical reflectance. It is also possible to compute directional-hemispherical reflectance, equivalent to the hemispherical directional reflectance in this case, thanks to the reversibility of light principle.

4.1 Angular Reflectance

Let us consider that the cavity is illuminated over a band of width Δx along the x axis, perpendicular to the cavity, i.e. illuminated along the y axis, by collimated light from a direction (θ, φ). The illumination is uniform, i.e., same radiance L_i arrives in each point of the band, which receives a uniform irradiance

$$E_i = L_i \cos\theta_i \Delta\omega_i \tag{20}$$

where $\Delta\omega_i$ denotes the small solid angle of illumination. Since the illuminated area is $2\sin(\alpha/2)\Delta x$, the incident flux on the band is $F_i = 2\sin(\alpha/2)\Delta x E_i$. On each elementary area within the band, centered around the position and of size $\Delta x dy_P$, the elementary flux is $dF_i = \Delta x dy_P E_i$.

The different elementary fluxes are reflected in various directions according to the panel that each one meets first and the number of reflections. By collecting the whole reflected flux, in practice with a measurement device equipped with an integrating sphere, the captured flux F_R is given by

$$F_r = \Delta x E_i \int_{y_p=-\sin(\alpha/2)}^{\sin(\alpha/2)} R(\theta, \varphi, y) dy_P \tag{21}$$

The directional-hemispherical reflectance of the band, and by extension to the whole structured surface, associated with this orientation of the incident light, is therefore:

$$R(\theta, \varphi) = \frac{F_r}{F_i} = \frac{1}{2\sin(\alpha/2)} \int_{y_p=-\sin(\alpha/2)}^{\sin(\alpha/2)} R(\theta, \varphi, y) dy_P \tag{22}$$

Again, according to the Helmholtz reciprocity principle, the angular function $R(\theta, \varphi)$ given by Eq. (22) also corresponds to the hemispherical-directional reflectance function of the structured surface when it is illuminated by Lambertian light over the hemisphere (same radiance L_i comes from every direction) and observed in the direction (θ, φ).

Notice that since the specular reflections on the panels do not modify the geometrical extent of the rays, the radiance L_r perceived in one direction (θ_r, φ_r) is:

$$L_r(\theta_r, \varphi_r) = R(\theta_r, \varphi_r) L_i \tag{23}$$

It is possible to display the reflectance given by Eq. (22) according to the observation direction on a 2D map thanks to the Lambert azimuthal equal area projection. To every direction (θ, φ) corresponds a point (u, v) within a disk of radius $\sqrt{2}$ whose coordinates are given by:

$$\begin{cases} u = 2\sin(\theta/2)\cos\varphi \\ v = 2\sin(\theta/2)\sin\varphi \end{cases} \tag{24}$$

The advantage of this transformation is that it conserves the areas by mapping a portion of the hemisphere of a given area, into a portion of the disk with same area.

In Fig. 5, we present the results given by Eq. (22) for two different materials, for aperture angle values of 45, 60, 90, 120, 150° and 180°. One material is dielectric, with a refraction index of 1.5. Its spectral reflectances are converted first in CIE 1931 XYZ tristimulus values then into L*a*b* color values, for a better visualization. The other one is made of copper, with tabulated values for the refractive index in the visible spectrum of light (400–700 nm), the spectral reflectances being converted in CIE 1931 XYZ tristimulus values, and then into sRGB color values.

For the dielectric material, we can see that the reflectance is globally very weak, except at high incidence angles (periphery of the graphs) when the cavity aperture angle is large. This is coherent with the angular variations of the Fresnel formulae. The highest angular reflectances peaks are located near the zones where the azimuthal angle $\varphi = \pi/2$, i.e. when the incident plane contains the x-axis. We can also see that the

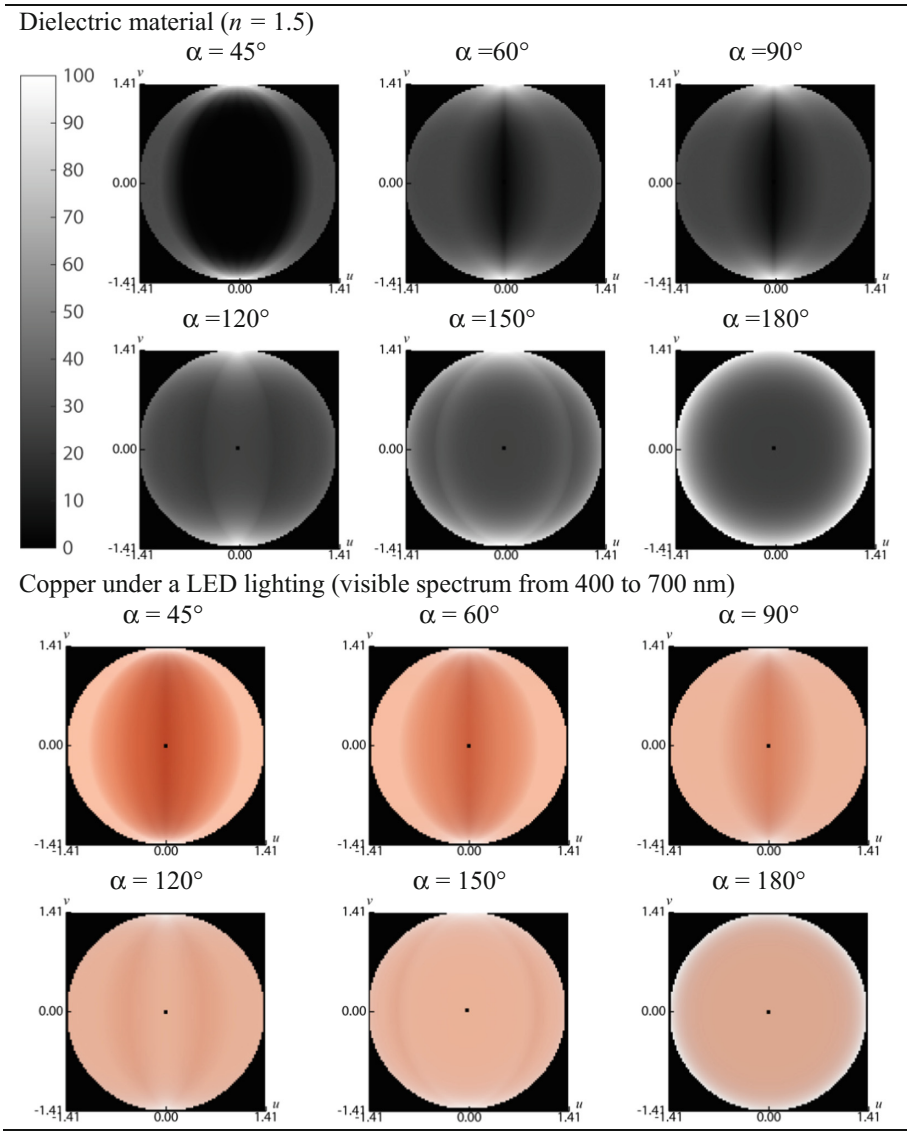

Fig. 5. Maps of hemispherical-directional reflectance (in %) for cavities of dielectric material, and color maps for cavities of copper, obtained with different aperture angles of cavities, represented with the Lambert azimuthal equal area projection.

radiance gradients have some discontinuities, which correspond to the directions at which the number of reflections within the cavity is incremented by one. For example, on the map attached to an aperture of 120°, a central area is lighter than the rest of the graph: it corresponds to rays undergoing one reflection, whereas in the rest of the graphs, rays undergo two reflections.

It is even more visible in the case of the copper. This material being more reflective, the reflected light appears more sliced into specific areas. It is also important to notice the saturation of the color increasing when the aperture angle decreases, as also shown in the case of diffusing surfaces in [20].

4.2 Bi-Hemispherical Reflectance

Now, we want to investigate the bi-hemispherical reflectance of the V-cavity and the influence of the surface structure (aperture angle α).

The bi-hemispherical reflectance corresponds to a uniform illumination over the hemisphere (Lambertian illumination, characterized by a constant radiance L_i from every direction), and a capture of the whole reflected light over the hemisphere. It is obtained by integrating over the hemisphere the angular reflectance studied previously, as follows.

The irradiance on the structured surface is related to the radiance L_i by:

$$E_i = \int_{\theta=0}^{\pi/2} \int_{\varphi=0}^{2\pi} L_i \cos\theta \sin\theta d\theta d\varphi = \pi L_i \tag{25}$$

and the incident flux on a band of the $2\sin(\alpha/2)\Delta x$ area cavity is:

$$F_i = 2\sin(\alpha/2)\Delta x E_i \tag{26}$$

The exitance is the sum of the reflected radiances expressed by Eq. (23):

$$M = \int_{\theta_r=0}^{\pi/2} \int_{\varphi_r=0}^{2\pi} L_r(\theta_r, \varphi_r) \cos\theta_r \sin\theta_r d\theta_r d\varphi_r \tag{27}$$

where $L_r = R(\theta_r, \varphi_r)L_i$ is the radiance reflected by the cavity according to the reflectance defined by Eq. (22).

Finally, the bi-hemispherical reflectance is given by:

$$R = \frac{M}{E_i} = \frac{1}{\pi L_i} \int_{\theta_r=0}^{\pi/2} \int_{\varphi_r=0}^{2\pi} L_r(\theta_r, \varphi_r) \cos\theta_r \sin\theta_r d\theta_r d\varphi_r \tag{28}$$

which yields, according to Eqs. (20) and (21),

$$R = \frac{1}{2\pi \sin(\alpha/2)} \int_{\theta_r=0}^{\pi/2} \int_{\varphi_r=0}^{2\pi} \int_{y_p=-\sin(\alpha/2)}^{\sin(\alpha/2)} R(\theta_r, \varphi_r, y) dy_P \cos\theta_r \sin\theta_r d\theta_r d\varphi_r \quad (29)$$

Using Eq. (29), we computed the bi-hemispherical reflectances for various aperture angles of the specular V-cavity, for the dielectric material previously studied, and for a cavity of silver at 550 nm ($n = 0.1249 + i3.3391$). The values are presented in Table 1.

Table 1. Bi-hemispherical reflectances for various cavity aperture angles.

Aperture angle	45°	60°	90°	120°	150°	180°
Silver	0.87	0.91	0.94	0.95	0.96	0.97
Dielectric ($n = 1.5$)	0.01	0.02	0.04	0.05	0.08	0.09

The bi-hemispherical values in Table 1 confirm the tendencies drawn by the angular reflectance maps. As the aperture angle gets smaller, the reflectance is lower and the structured surface has a darker appearance, which is due to the increase of the number of light reflections in the cavities, each reflection introducing a radiance attenuation. It is illustrated by Table 2, where we computed, in the case of a cavity of silver at 550 nm ($n = 0.1249 + i3.3391$) with an aperture of 45°, the bi-hemispherical reflectance by taking into account only 1 light reflections, then adding the paths of the light where a second reflection happens, then a third one, up to the maximum number of 4 light reflections possible in this structure.

Table 2. Bi-hemispherical reflectance of a 45° V-cavity made of silver at 550 nm

Maximal number of light reflections	Bi-hemispherical reflectance
1	0.14
2	0.40
3	0.70
4	0.97

We observe from these results that if we take into account only one or two light reflections, as it is often done in light scattering models by rough metallic surfaces, we underestimate the reflectance. The error is sensible in the case of media with high refractive index, like metals. It is also visible through Fig. 6, where the angular reflectance for silver at 550 nm with an aperture of 45° is represented in the cases where we only consider one reflection of the light, or all the possible reflections.

In order to obtain a more precise prediction of the appearance, especially in the case of a small aperture angle in the concavities of the surface topography, it is necessary to compute it with a sufficient number of light reflections, as also shown recently in the domain of computer graphics [10, 11].

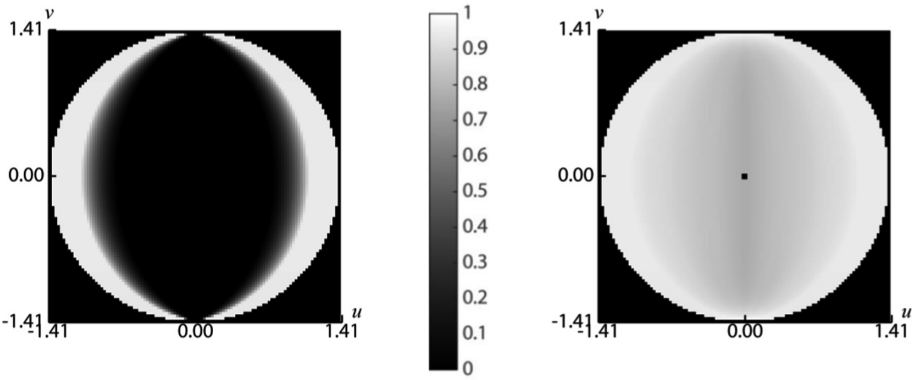

Fig. 6. Maps of angular reflectance for a 45° V-cavity made of silver, at 550 nm ($n = 0.1249 + i3.3391$), represented with the Lambert azimuthal equal area projection, where only one reflection (left) and all the possible reflections (right) of rays in the cavity are rendered.

5 Conclusions

In this paper, we analyzed the interreflections happening in a structured surface made of parallel, specular V-cavities under a Lambertian illumination. We proposed a model taking into account the exact number of light reflections occurring in the structures, in order to accurately predict the reflectance according to the observation angle. We saw that the material and the angle of the cavity have a strong impact on the interreflections and the reflectance of the concave surfaces, in particular because of the number of light reflections. We also showed that it is crucial to model correctly the number of light reflections happening in surfaces presenting concavities with small aperture angle, as it has a great influence on the final visual appearance. This constitutes an extension for the modelization of the light being reflected by complex surfaces, to better predict the visual appearance of given surfaces. It could be combined in the future with a model predicting the interreflections in similar cavities made of a Lambertian material, in order to predict the appearance of a diffusing material presenting a structured interface with air.

References

1. Kinoshita, S., Yoshioka, S., Miyazaki, J.: Physics of structural colors. Rep. Prog. Phys. **71**, 076401 (2008)
2. Charrière, R., Lacaille, G., Pedeferri, M., Faucheu, J., Delafosse, D.: Characterization of the gonioapparent character of colored anodized titanium surfaces. Color Res. Appl. **40**(5), 483–490 (2015)
3. Kubelka, P.: New contributions to the optics of intensely light-scattering material. Part I. J. Opt. Soc. Am. A **38**, 448–457 (1948)
4. Melamed, N.T.: Optical properties of powders: Part I. optical absorption coefficients and the absolute value of the diffuse reflectance. J. Appl. Phys. **34**, 560–570 (1963)
5. Chandrasekhar, S.: Radiative Transfer. Dover, Illinois (1960)
6. van de Hulst, H.C.: Light Scattering by Small Particles, pp. 200–227. Dover, Illinois (1981)
7. Beckmann, P., Spizzichino, A.: The Scattering of Electromagnetic Waves from Rough Surfaces, pp. 70–98. MA Artech House Inc, Norwood (1963)
8. Torrance, K.E., Sparrow, E.M.: Theory for off-specular reflection from roughened surfaces. J. Opt. Soc. Am. **57**(9), 1105–1114 (1967)
9. Heitz, E., Hanika, J., d'Eon, E., Dachsbacher, C.: Multiple-scattering microfacet BSDFs with the Smith model. ACM Trans. Graph. **35**(4) (2016). Proceedings of the SIGGRAPH 2016. Article 58
10. Lee, J.H., Jarabo, A., Jeon, D.S., Gutierrez, D., Kim, M.H.: Practical multiple scattering for rough surfaces. In: SIGGRAPH Asia 2018 Technical Papers, p. 275. ACM (2018)
11. Xie, F., Hanrahan, P.: Multiple scattering from distributions of specular v-grooves. In: ACM SIGGRAPH Asia, p. 276 (2018)
12. Kubelka, P.: New contributions to the optics of intensely light-scattering materials. Part II: non homogeneous layers. J. Opt. Soc. Am. A **44**, 330–335 (1954)
13. Simonot, L., Hébert, M., Hersch, R.D.: Extension of the Williams-Clapper model to stacked nondiffusing colored coatings with different refractive indices. J. Opt. Soc. Am. A **23**, 1432–1441 (2006)
14. Hébert, M., Hersch, R.D., Becker, J.-M.: Compositional reflectance and transmittance model for multilayer specimens. J. Opt. Soc. Am. A **24**, 2628–2644 (2007)
15. Emmel, P., Hersch, R.D.: A unified model for color prediction of halftoned prints. J. Im. Sci. Technol. **44**(4), 351–359 (2000)
16. Clapper, F.R., Yule, J.A.C.: The effect of multiple internal reflections on the densities of halftone prints on paper. J. Opt. Soc. Am. **43**, 600–603 (1953)
17. Yule, J.A.C., Nielsen, W.J.: The penetration of light into paper and its effect on halftone reproductions. In: Proceedings of the TAGA, vol. 3, pp. 65–76 (1951)
18. Rogers, G.: Effect of light scatter on halftone color. J. Opt. Soc. Am. A **15**, 1813–1821 (1998)
19. Rogers, G.: A generalized clapper-yule model of halftone reflectance. Color Res. Appl. **25**, 402–407 (2000)
20. Saint-Pierre, D., Deeb, R., Muselet, D., Simonot, L., Hébert,M.: Light interreflections and shadowing effects in a Lambertian V-cavity under diffuse illumination. In: IS&T Electronic Imaging Symposium, Material Appearance, Burlingame, USA, 29 January–2 February 2018
21. Deeb, R., Muselet, D., Hebert, M., Trémeau, A.: Spectral reflectance estimation from one RGB image using self-interreflections in a concave object. Appl. Opt. **57**(17), 4918–4929 (2018)